Localized Plasticity and Associated Cracking in Stable and Metastable High-Entropy Alloys Pre-Charged with Hydrogen

As Published: 10.1016/J.PROSTR.2018.12.119

Publisher: Elsevier BV

Persistent URL: https://hdl.handle.net/1721.1/135071

Version: Final published version: final published article, as it appeared in a journal, conference proceedings, or other formally published context

Available online at www.sciencedirect.com

ScienceDirect

Procedia Structural Integrity 13 (2018) 716–721

Structural Integrity Procedia

www.elsevier.com/locate/procedia

ECF22 - Loading and Environmental effects on Structural Integrity

Localized Plasticity and Associated Cracking in Stable and Metastable High-Entropy Alloys Pre-Charged with Hydrogen

Kenshiro Ichii [a], Motomichi Koyama [a], Cemal Cem Tasan [b], Kaneaki Tsuzaki [a, c]

[a] *Department of Mechanical Engineering, Kyushu University, Japan*
[b] *Department of Materials Science and Engineering, Massachusetts Institute of Technology, USA*
[c] *Hydrogenious, Kyushu University, Japan*

Abstract

We investigated hydrogen embrittlement in Fe20Mn20Ni20Cr20Co and Fe30Mn10Cr10Co (at.%) alloys pre-charged with 100 MPa hydrogen gas by tensile testing at three initial strain rates of 10^{-4}, 10^{-3}, and 10^{-2} s^{-1} at ambient temperature. The alloys are classified as stable and metastable austenite-based high-entropy alloys (HEAs), respectively. Both HEAs showed the characteristic hydrogen-induced degradation of tensile ductility. Electron backscatter diffraction analysis indicated that the reduction in ductility by hydrogen pre-charging was associated with localized plasticity-assisted intergranular crack initiation. It should be noted as an important finding that hydrogen-assisted cracking of the metastable HEA occurred not through a brittle mechanism but through localized plastic deformation in both the austenite and ε-martensite phases.

Peer-review under responsibility of the ECF22 organizers.

Keywords: High-entropy alloy; Hydrogen embrittlement; Martensitic transformation; Austenitic steels; Hydrogen desorption

1. Introduction

High-entropy alloys (HEA) are now one of the most focused alloy groups in the field of materials science and engineering because of their marked property improvements, e.g., combined strength and ductility (Zhang et al., 2014) and cryogenic fracture resistance (Gludovatz et al., 2014). As has been reported in steels, the reduction in phase stability of austenite in HEAs was reported to improve their tensile properties through the transformation-induced plasticity (TRIP) effect (Li et al., 2016). It is interesting to note that the TRIP effect in HEAs arises from the ε-martensitic transformation from a face-centered cubic (FCC) to a hexagonal close-packed (HCP) phase, and not from the α′-martensitic transformation from a FCC to a body-centered cubic (BCC) phase (Li et al., 2016, Li et al., 2017).

In recent studies, a Fe20Mn20Ni20Cr20Co HEA with stable austenite was reported to show high hydrogen embrittlement resistance (Zhao et al., 2017); hydrogen introduction instead showed a positive effect on elongation and

2452-3216
Peer-review under responsibility of the ECF22 organizers.
10.1016/j.prostr.2018.12.119

strength (Luo et al., 2017). These results are in good agreement with those for conventional austenitic steels (Michler et al., 2012, Astafurova et al., 2010, Yamada et al., 2015). In general, stable austenitic steels with low hydrogen diffusivities show low susceptibilities to hydrogen embrittlement. The positive effect of hydrogen on tensile ductility was reported for a high-Mn austenitic steel and attributed to the formation of deformation twins (Astafurova et al., 2010, Yamada et al., 2015). Furthermore, even if the austenite is unstable, the effect of the ε-martensitic transformation is not fatal for susceptibility to hydrogen embrittlement compared to the case of α′-martensitic transformation (Tsuzaki et al., 2016, Koyama et al., 2017). The hydrogen embrittlement resistance in the ε-phase partially arises from its lower hydrogen diffusivity than that in the BCC or even FCC phases (He et al., 2017, Hirata et al., 2018).

These recent studies indicate that the HEA concept provides a new class of hydrogen-resistant structural materials. Hence, we investigate the hydrogen embrittlement susceptibility by introducing hydrogen in the form of a 100 MPa high-pressure gas. Note that this is one of the most severe conditions for hydrogen-energy-related infrastructures.

2. Material and Methods

Two types of HEAs are prepared: Fe20Mn20Ni20Cr20Co and Fe30Mn10Cr10Co (at.%). Table 1 shows the details of the chemical compositions of the HEAs. The former is a HEA with stable austenite and is referred to as the stable HEA, while the latter exhibits a dual-phase microstructure consisting of metastable austenite and ε-martensite and is referred to as the metastable HEA. The metastable HEA shows the TRIP effect arising from the ε-martensitic transformation, as mentioned above (Li et al., 2016, Li et al., 2017). Ingots of 50 kg in mass of the two alloys were prepared by vacuum induction melting. The ingots were hot-rolled to 52% thickness at 1273 K followed by homogenization at 1473 K for 2 h in an Ar atmosphere and then furnace-cooling. The homogenized bars were further hot-rolled to obtain a thickness reduction to 33% from 60 to 20 mm. The rolled bars were solution-treated at 1073 K in an air atmosphere for 1 h, followed by water-quenching. Tensile specimens of 1 mm in thickness were made by electric discharge machining. The gauge length and width of the specimens were 10 mm and 2 mm, respectively. For hydrogen pre-charging, the specimens were exposed to a 100 MPa hydrogen gas atmosphere at 543 K for 200 h. Tensile testing was performed in air at ambient temperature (293 K) and at three initial strain rates of 10^{-4}, 10^{-3}, and 10^{-2} s^{-1}. After the tensile tests, the microstructures and fracture surfaces were examined by electron backscatter diffraction (EBSD) and secondary electron imaging, respectively. The EBSD measurements were conducted at 20 kV and a beam step size of 50 nm after mechanically polishing the specimen surface. The fracture surface observations were performed at 15 kV.

Table 1. Chemical compositions of the high entropy alloys (HEAs) (mass %).

Steels	C	Mn	P	S	N	O	Al	Cr	Co	Ni	Fe
Stable HEA	0.002	19.77	0.002	0.006	0.0065	0.007	0.018	18.23	20.85	20.21	20.90
Metastable HEA	0.009	29.80	0.004	0.007	0.0087	0.015	0.028	9.29	10.46	0.01	50.37

3. Results and Discussion

3.1. Hydrogen absorption

We measured the diffusible hydrogen content by thermal desorption spectroscopy at a heating rate of 400 K h^{-1}. The results are listed in Table 2 (Ichii et al., 2018). The diffusible hydrogen contents of the stable and metastable HEAs, defined as the cumulative hydrogen contents from 313 to 873 K, were determined to be 113 and 178 mass ppm, respectively. It was suggested in our previous paper (Ichii et al., 2018) that the higher diffusible hydrogen content of the metastable HEA may relate to the presence of thermally induced ε-martensite with stacking faults and HCP/FCC interfaces. However, here we must note that the hydrogen charging temperature of 543 K is higher than the A_f temperature (the finish temperature of the HCP-to-FCC reverse transformation) of the present metastable HEA. Thus, the difference in the measured hydrogen content must be associated with the state of the austenite matrices in the alloys, e.g., their chemical compositions or lattice defects such as dislocations and stacking faults formed by the HCP-to-FCC reverse transformation during heating to 543 K. It should be understood from Table 2 that large hydrogen contents of >100 mass ppm were absorbed into both alloys by the 100 MPa hydrogen gas charging.

Table 2. The diffusible hydrogen content and desorption peak temperature obtained by the thermal desorption spectroscopy.

	Diffusible hydrogen content	Peak temperature
Stable HEA	113 mass ppm	512 K
Metastable HEA	178 mass ppm	564 K

3.2. Tensile properties

Fig. 1 shows the engineering stress–strain curves of (a) the stable HEA and (b) the metastable HEA with and without hydrogen charging. Zhao et al. (2017) had performed tensile testing at an initial strain rate of 10^{-4} s^{-1} for the stable HEA pre-charged with a 10 MPa hydrogen gas atmosphere, which caused no hydrogen embrittlement. On the other hand, in both the stable and metastable HEAs, the severe hydrogen charging conditions using a 100 MPa hydrogen gas pressure significantly decreased the tensile ductility. It is also noted that the tensile ductility is recovered very slightly with increasing strain rate and that the hydrogen uptake increases the yield strength, perhaps through solution hardening by the hydrogen. We note the following two facts. (1) While the previous work (Zhao et al., 2017) with a 10 MPa hydrogen gas pressure yielded no hydrogen embrittlement, hydrogen embrittlement occurs even in the stable HEA when hydrogen is introduced at 100 MPa. (2) Both HEAs with hydrogen charging exhibit similar tensile strengths, although the hydrogen content in the metastable HEA is higher than that in the stable HEA.

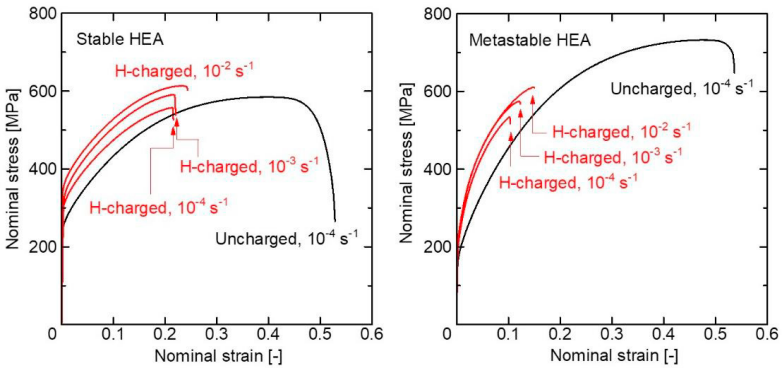

Fig. 1. Engineering stress-strain curves of the (a) stable and (b) metastable HEAs with and without 100 MPa hydrogen gas pre-charging.

3.3. Hydrogen-assisted cracking and failure

Fig. 2 shows scanning electron microscopy (SEM) images of the broad surfaces near the failure portions of the specimens tested at the initial strain rate of 10^{-4} s^{-1} (a, d) without and (b, e) with hydrogen pre-charging. Figs. 2(b) and (e) reveal slight necking in both HEAs with hydrogen pre-charging. Furthermore, it should be noted that subcracks are seen on the broad surfaces only in the hydrogen-charged specimens, as indicated in Figs. 2(c) and (f). EBSD images around the subcracks of the fractured specimens at the initial strain rate of 10^{-4} s^{-1} with hydrogen charging are shown in Fig. 3. They indicate that both the stable and metastable HEAs exhibit intergranular crack initiation with orientation rotation. The grain reference orientation deviation (GROD) mapping in Figs. 3(d) and (h) shows relatively high GROD values at the grain boundaries. This suggests that the subcracks are initiated with the formation of the orientation gradient. This fact also indicates that localized plastic deformation assists intergranular crack initiation.

For the metastable HEA, it is interesting to note that both the austenite and ε-martensite are locally plastically deformed around the intergranular crack, as shown in Figs. 3(g) and (h). In general, ε-martensite causes brittle-like cracking because of the limited number of slip systems in the HCP structure. However, as seen in the GROD map in Fig. 3(h), hydrogen-assisted cracking occurs by a ductile mechanism associated with local plasticity. This strongly suggests that the increase in configurational entropy provides the high ductility of ε-martensite. Hence, the hydrogen-charged metastable HEA showed similar tensile strength even with the higher diffusible hydrogen content compared to the hydrogen-charged stable HEA.

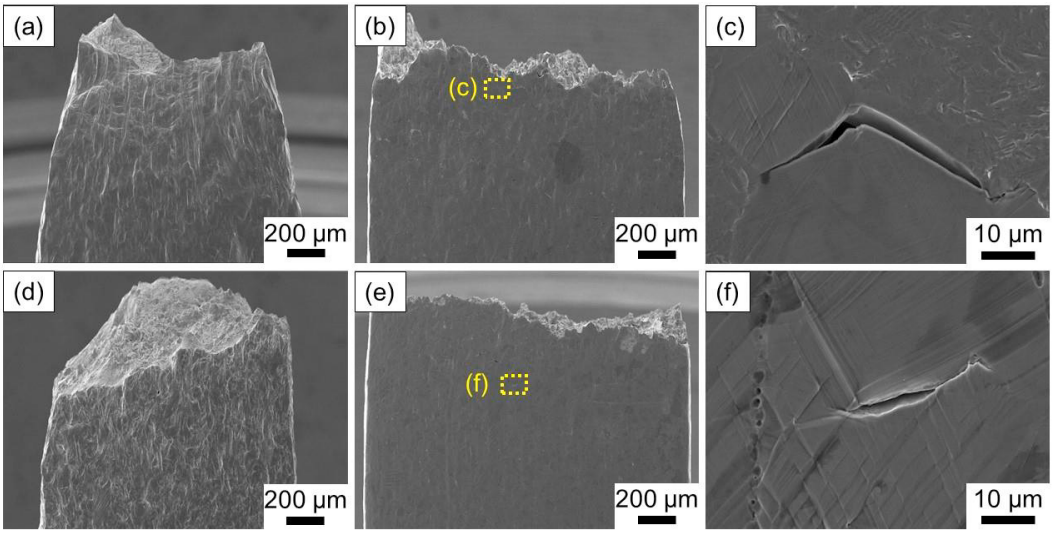

Fig. 2. SEM images of the specimen surfaces near the failure portions for (a-c) the stable and (d-f) metastable HEAs. (a) and (d): without hydrogen gas pre-charging. (b, c) and (e, f): with hydrogen gas pre-charging. (c) and (f) are the magnified images of the rectangle region indicated in (b) and (e) respectively. The initial strain rate was 10^{-4} s^{-1}. Secondary electron images were taken at 15 kV.

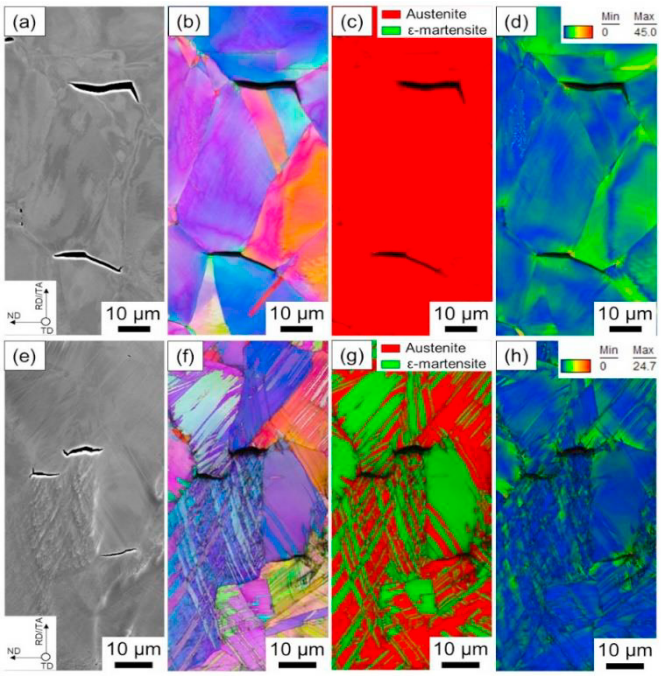

Fig. 3. Surface cracks and corresponding EBSD images of the (a–d) stable and (e–h) metastable high entropy alloys. (a, e) Secondary electron images; (b, f) rolling direction - inverse pole fig. (RD-IPF) maps; (c, g) phase maps; (d, h) GROD maps. The initial strain rate is 10^{-4} s^{-1}. The tensile direction is vertical.

For a more detailed discussion, we observed the fracture surfaces by SEM. Fig. 4 shows the results for the (a, c) stable and (b, d) metastable HEAs (a, b) without and (c, d) with hydrogen charging. The fracture surfaces of both the stable and metastable HEAs without hydrogen charging consist of dimples, as seen in Figs. 4(a) and (b), indicating that ductile fracture occurred. In contrast, an intergranular fractured surface is observed in both the stable and metastable HEAs with hydrogen pre-charging. In addition, the hydrogen-charged metastable HEA shows considerable

slip traces on the fracture surface (Fig. 4 (d)). This indicates slip localization-assisted damage evolution along the grain boundaries (Koyama et al., 2014). Furthermore, while quasi-cleavage cracking is not observed on the specimen's broad surface (Figs. 3(e–h)), step-like ridges are recognized on the fracture surface (Fig. 4(d)). This suggests that the surface cracking occurred at the grain boundaries while the quasi-cleavage cracking happened during the crack propagation process until failure.

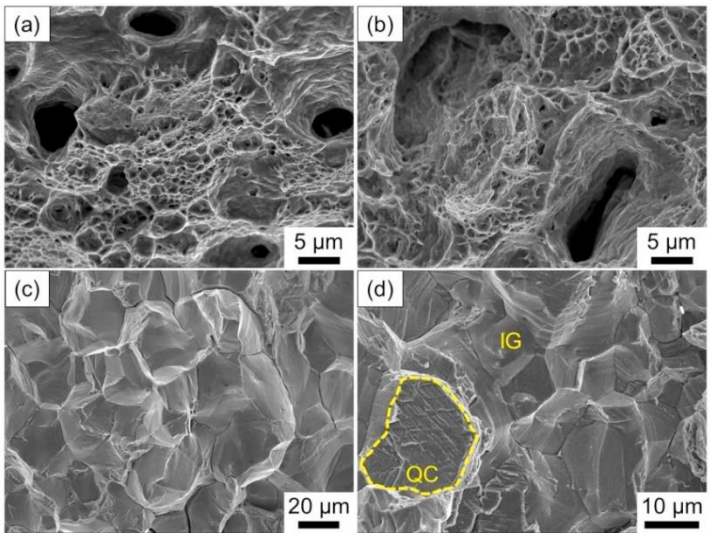

Fig. 4. Fractographs of (a, c) the stable and (b, d) metastable high entropy alloys (a, b) without and (c, d) with hydrogen charging. The initial strain rate is 10^{-4} s^{-1}. IG: intergranular region, QC: quasi-cleavage region.

Consequently, both the intergranular and transgranular cracking mechanisms are enhanced by localized plasticity in the metastable HEA with hydrogen charging, thus assisting ductile fracture along grain boundaries. More specifically, the ductility of the ε-martensite is necessary to understand the underlying mechanism of the hydrogen-assisted failure of the metastable HEA. In addition, the competitive motion of dislocations and diffusible hydrogen is important in the context of the strain rate effect in the metastable HEA. That is, the dislocation velocity becomes significantly higher than hydrogen diffusion with increasing strain rate, which suppresses localized plasticity and associated ductile damage evolution.

4. Conclusion

We investigated hydrogen embrittlement in Fe20Mn20Ni20Cr20Co and Fe30Mn10Cr10Co (at.%) alloys by tensile testing at three initial strain rates of 10^{-4}, 10^{-3}, and 10^{-2} s^{-1} at ambient temperature. Hydrogen was introduced with 100-MPa hydrogen gas before the tensile tests. The following conclusions are obtained.

- Both the stable and metastable HEAs showed distinct hydrogen-assisted failures after exposure to the 100-MPa hydrogen gas at the initial strain rates of 10^{-4}, 10^{-3}, and 10^{-2} s^{-1}. In both the HEAs, localized plasticity was important in elucidating the hydrogen embrittlement mechanisms.
- Although the metastable HEA with hydrogen charging showed a degradation in tensile ductility, its tensile strength was comparable to that of the stable HEA, owing to the high plastic deformability of ε-martensite. In other words, the increase in configurational entropy tended to cause an improvement in the ductility of ε-martensite, even with the negative effects of hydrogen.

5. Acknowledgements

This work was financially supported by JSPS KAKENHI (JP16H06365 and JP17H04956) and the Japan Science and Technology Agency (JST) (grant number: 20100113) under Industry-Academia Collaborative R&D Program.

6. References

Astafurova, E.G., Zakharova, G.G., Maier, H.J., 2010. Hydrogen-induced twinning in <0 0 1> Hadfield steel single crystals. Scr. Mater. 63, 1189–1192.

Gludovatz, B., Hohenwarter, A., Catoor, D., Chang, E.H., George, E.P., Ritchie, R.O., 2014. A fracture-resistant high-entropy alloy for cryogenic applications. Science. 345, 1153–1158.

He, Y., Li, Y., Chen, C., Yu, H., 2017. Diffusion coefficient of hydrogen interstitial atom in α-Fe, γ-Fe and ε-Fe crystals by first-principle calculations. Int. J. Hydrogen Energy 42, 27438–27445.

Hirata, K., Iikubo, S., Koyama, M., Tsuzaki, K., Ohtani, H., 2018. First-principles study on hydrogen 1 diffusivity in BCC, FCC, and HCP iron. Metal. Mater. Trans. A, accepted.

Koyama, M., Akiyama, E., Lee, Y.-K., Raabe, D., Tsuzaki, K., 2017. Overview of hydrogen embrittlement in high-Mn steels. Int. J. Hydrogen Energy 42, 12706–12723.

Koyama, M., Springer, H., Merzlikin, S. V., Tsuzaki, K., Akiyama, E., Raabe, D., 2014. Hydrogen embrittlement associated with strain localization in a precipitation-hardened Fe–Mn–Al–C light weight austenitic steel. Int. J. Hydrogen Energy 39, 4634–4646.

Li, Z., Pradeep, K.G., Deng, Y., Raabe, D., Tasan, C.C., 2016. Metastable high-entropy dual-phase alloys overcome the strength-ductility trade-off. Nature 534, 227–230.

Li, Z., Tasan, C.C., Pradeep, K.G., Raabe, D., 2017. A TRIP-assisted dual-phase high-entropy alloy: Grain size and phase fraction effects on deformation behavior. Acta Mater. 131, 323–335.

Luo, H., Li, Z., Raabe, D., 2017. Hydrogen enhances strength and ductility of an equiatomic high-entropy alloy. Sci. Rep. 7, 1–7.

Michler, T., San Marchi, C., Naumann, J., Weber, S., Martin, M., 2012. Hydrogen environment embrittlement of stable austenitic steels. Int. J. Hydrogen Energy 37, 16231–16246.

Tsuzaki, K., Fukuda, K., Koyama, M., Matsunaga, H., 2016. Hexagonal close-packed Martensite-related Fatigue Crack Growth under the Influence of Hydrogen: Example of Fe-15Mn-10Cr-8Ni-4Si Austenitic Alloy. Scr. Mater. 113, 6–9.

Yamada, K., Koyama, M., Kaneko, T., Tsuzaki, K., 2015. Positive and negative effects of hydrogen on tensile behavior in polycrystalline Fe–30Mn–(6−x)Si–xAl austenitic alloys. Scr. Mater. 105, 54–57.

Zhang, Y., Zuo, T.T., Tang, Z., Gao, M.C., Dahmen, K.A., Liaw, P.K., Lu, Z.P., 2014, Microstructures and properties of high-entropy alloys, Progress in Materials Science 61, 1–93.

Zhao, Y., Lee, D.-H., Seok, M.-Y., Lee, J.-A., Phaniraj, M.P., Suh, J.-Y., Ha, H.-Y., Kim, J.-Y., Ramamurty, U., Jang, J., 2017. Resistance of CoCrFeMnNi high-entropy alloy to gaseous hydrogen embrittlement. Scr. Mater. 135, 54–58.